AIAA JOURNAL
Vol. 33, No. 9, September 1995

Numerical/Experimental Study of a Wingtip Vortex in the Near Field

Jennifer Dacles-Mariani* and Gregory G. Zilliac†
NASA Ames Research Center, Moffett Field, California 94035
and
Jim S. Chow‡ and Peter Bradshaw§
Stanford University, Stanford, California 94305

The near-field behavior of a wingtip vortex flow has been studied computationally and experimentally in an interactive fashion. The computational approach involved using the method of artificial compressibility to solve the three-dimensional, incompressible, Navier–Stokes equations with experimentally determined boundary conditions and a modified Baldwin–Barth turbulence model. Inaccuracies caused by the finite difference technique, grid resolution, and turbulence modeling have been explored. The complete geometry case was computed using 1.5 million grid points and compared with mean velocity measurements on the suction side of the wing and in the near wake. Good agreement between the computed and measured flowfields has been obtained. The velocity distribution in the vortex core compares to within 3% of the experiment.

I. Introduction

AT some point in the not so distant future, it will be possible to compute the three-dimensional viscous flowfield around a Boeing 747 under cruise conditions with an accuracy of 0.5% in a day. This feat will most likely be accomplished using a Reynolds-averaged Navier–Stokes solver on a computer with the capability of $\mathcal{O}(10^{14})$ FLOPs and $\mathcal{O}(10^{12})$ words of memory [estimate based on $\mathcal{O}(h^2)$ solver, $Re_c = 70 \times 10^6$, where Re_c is the Reynolds number based on chord length, extrapolation of the current state-of-the-art full aircraft computations and predicated on the assumption that it is possible to reduce turbulence modeling errors to less than 0.5%]. Development of this capability would put the computer on a par with the best wind tunnels for full aircraft configuration studies. The pacing items in computational fluid dynamics (CFD) for aerodynamic calculations are supercomputer development, solver accuracy, grid generation, and turbulence modeling. In these four areas, many advances have been made, but the fact remains that most wing computations are, at best, 5% accurate (in drag coefficient, for example). This level of accuracy has been sufficient for many purposes such as airfoil design, rudimentary wing design, and some forms of optimization. However, this accuracy level will not allow commercial aircraft designers to extract the remaining few percent of efficiency theoretically possible for conventional aircraft configurations.

In the present study, we have combined experiment and computation with the hope that we could accurately measure, compute, and validate a high-Reynolds-number wing flowfield. We have also attempted to isolate the roles of solver accuracy, grid resolution, and turbulence modeling, in obtaining accurate computations.

Two computational studies[1,2] have been completed that have direct relevance to the present study. The numerical work done by Mansour[1] was one of the first attempts at using an implicit, three-dimensional thin-layer Navier–Stokes solver to compute the flow around a transonic swept wing. His calculations indicated that the flow around the wing leading edge has a significant impact on the tip-vortex formation for this swept wing. However, his calculations predicted the leading-edge suction peak, shock location, and shock strength to be significantly different from measured results of Keener. Srinivasan et al.[2] performed a numerical study of the effect of tip-planform and tip-cap shape on the formation and roll-up of a vortex. Good qualitative comparisons with experimental work by Spivey and Moorehouse[3] was obtained. However, the computed viscous wake region and the vortex-induced surface-pressure suction peak on the tip were not well resolved. Inaccuracies in these computational studies can be attributed to numerical errors and errors owing to transition/turbulence modeling.

Accurate finite difference computations of vortical flows require resolution of not only the viscous boundary-layer region but also other areas with high flow gradients such as in the vicinity of the vortex core [the core is defined as the region from $v_\theta = 0$ in the center of the vortex to maximum v_θ where v_θ is defined as the circumferential velocity component] and the near-field wake region. For these reasons, sufficient grid density and appropriate distribution are essential. The inaccuracy caused by poor grid resolution manifests itself in the form of excessive numerical dissipation. Thus, use of high-order accurate discretization is important. Since wingtip vortices can persist for hundreds of wing-chord lengths, proper treatment of boundary conditions is also of importance. The flowfield generated by a wingtip is often turbulent and highly three dimensional with the existence of local separation and secondary flows.[4] To date, development of a turbulence model that can accurately predict such complex flowfields has not been achieved.

The goal of this study is to accurately compute the formation of a turbulent wingtip vortex. The approach to this study is slightly different from most studies in that the experiment and computation have progressed in parallel and in a highly interactive fashion with substantial integration of the experimental data into the computation. For example, measured inflow and outflow boundary conditions have been used. To this end, several design choices were made to maximize the accuracy and usefulness of the results. Only one test case has been measured ($\alpha = 10$ deg and $Re_c = 4.6 \times 10^6$, with α being the angle of attack). It was decided that one thoroughly measured case was more desirable than several incomplete cases. Secondly, a high Reynolds number was chosen at the cost of large wind-tunnel blockage by the model (and very low aspect ratio). Since this is a generic model intended for code validation and since the interference is not large enough to alter the flow qualitatively (e.g., by causing boundary-layer separation), this flow, which has been documented in considerable detail, should be a representative test case

Received April 21, 1994; revision received Feb. 13, 1995; accepted for publication Feb. 13, 1995.

*NRC Associate, ADC Branch.
†Research Scientist, Fluid Mechanics Laboratory.
‡Doctoral Candidate; currently Research Staff Member, Institute for Defense Analysis.
§Professor. Member AIAA.

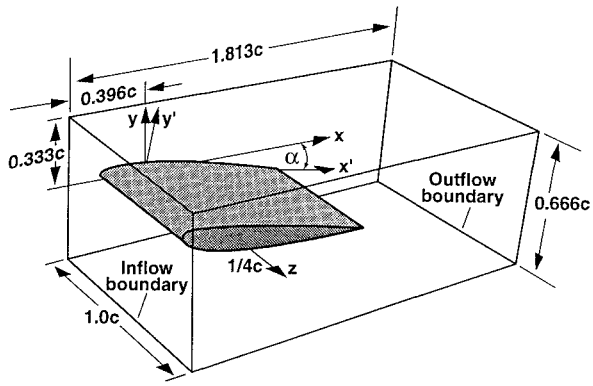

Fig. 1 Measurement and computational domain.

for present and future prediction methods. The main disadvantage is that the tunnel walls must be used as boundaries in a computation.

II. Procedure

Navier–Stokes Solver

A three-dimensional, incompressible Navier–Stokes flow solver, INS3D-UP,[6] was used in this study. This computer code has been successful in simulating aerodynamic as well as turbomachinery flow problems.[7,8] The flow code uses an implicit finite difference scheme in generalized curvilinear coordinates written in a primitive variable formulation. The algorithm is based on the artificial compressibility method.[9] A complete description of the numerical technique and the governing equations is presented in Refs. 6 and 7.

In a successful computation of the formation, growth, and decay of a vortex, the level of numerical dissipation should be orders of magnitude smaller than the dissipation caused by laminar diffusion. Higher order accurate differencing schemes have been shown to reduce dissipation errors (arising from truncation of the convective terms) considerably in vortex preservation tests[10] (i.e., tests that measure the ability of a computational method to predict the correct growth rate). Preliminary computations in the current study showed that a third-order accurate scheme was too dissipative. In the current application, an upwind-biased fifth-order accurate discretization of the convective terms, originally developed by Rai,[10] has been implemented. This differencing scheme uses a 7-point stencil as opposed to the 11-point stencil of a fully upwind scheme. The differencing of the viscous terms is second order.

Configuration

The geometry of what is referred to as the complete geometry case is a close approximation to the 32 × 48 in. low-speed wind tunnel and wing setup of Ref. 4. The model and coordinate system definitions are illustrated in Fig. 1. The model is a rectangular wing with a rounded tip and an aspect ratio of 0.75 of chord ($0.75c$). During preliminary computations, identification of the source of discrepancy between the computed and measured results proved to be difficult. It was apparent that the computed vortex was too diffused, but the origin of the false diffusivity could have been attributed to some combination of insufficient grid resolution, finite differencing method, turbulence modeling, grid-related numerical errors, or boundary conditions. Consequently, in addition to computation of the complete geometry case, a subset problem (the wake case) consisting of the region from the trailing edge to the outflow boundary and also an analytical vortex (the analytical vortex case) were studied. These cases enabled grid refinement and turbulence model testing to be done in a systematic and less costly manner.

Wake Case

The domain for the wake case included the region from the trailing edge to $0.69c$ downstream of the trailing edge. The experimental velocity profile in a crossflow plane at the trailing edge of the wing was imposed at the inflow. The inflow boundary condition for the pressure was computed based on the method of characteristics using one-dimensional Riemann invariants. The exit conditions were satisfied by prescribing an experimentally determined pressure distribution, whereas the velocity components at the outflow were calculated by using one-dimensional Riemann invariants. At the solid surface (wind-tunnel walls), the velocity was specified to be zero.

Analytical Vortex Case

In this case, the analytical, self-similar, free vortex solution of Rott[5] was used to investigate grid resolution. Rott's vortex is an exact solution to the Navier–Stokes equation. It is a steady, three-dimensional axisymmetric vortex similar to the unsteady Oseen vortex only frozen in time:

$$v_r = -ar$$

$$v_\theta = \frac{\Gamma_\infty}{(2\pi r)}\left(1 - e^{-ar^2/2\nu}\right)$$

$$v_x = 2ax$$

In the first equation, v_r is the velocity in the radial direction with a as the velocity gradient and r the radius. In the second equation, Γ_∞ is the vortex circulation in the freestream and ν is the kinematic viscosity. Finally, in the third equation, v_x is the velocity in the streamwise direction. The vortex is located on the centerline of the domain and extends downstream for about three core radii. The far-field boundaries extend from $-4.35r_c$ to $4.35r_c$ in the vertical and horizontal direction {with r_c being the core radius in the inflow}. This relatively small domain is similar in size to that of the wake case. The boundary conditions were determined from the analytical solution, and they were prescribed in a manner similar to the wake case.

Complete Geometry Case

The computational domain for this case included a rectangular half-wing with a NACA 0012 airfoil section, a rounded wing tip, and the surrounding boundaries as shown in Fig. 1. The wing has an aspect ratio of 0.75 and was mounted inside a wind tunnel at 10-deg angle of attack. The flow is turbulent with a Reynolds number of 4.6×10^6 based on the chord length. Boundary conditions imposed at the solid surfaces were similar to those of the wake case. The inflow and outflow boundary conditions were prescribed in the same manner as for the wake-case problem, although for some cases a Neumann outflow pressure boundary condition ($dP/d\psi$ as determined from measured data) was used.

Grid Generation

Several grid-generation strategies were explored in attempts to accurately resolve the flow on the wing and in the tip vortex. A single zone approach was considered to be preferable for this study (to avoid errors at zone boundaries); however, it is recognized that for more complex configurations a multizone approach is probably the only alternative. For the wake and analytical vortex cases, single grids (of sizes ranging from 16 × 21 × 21 to 16 × 81 × 81 points) were generated with uniformly distributed points in the region of the vortex. In the region between the vortex and the tunnel walls, the grid was stretched. Grid spacing sufficient to resolve the boundary layers on the tunnel wall was enforced. A single zone grid of C-O topology was used for the complete geometry case. The grid was a hybrid grid consisting of an inner hyperbolic grid generated using HYPGEN[11] surrounding the wing matched with an elliptic

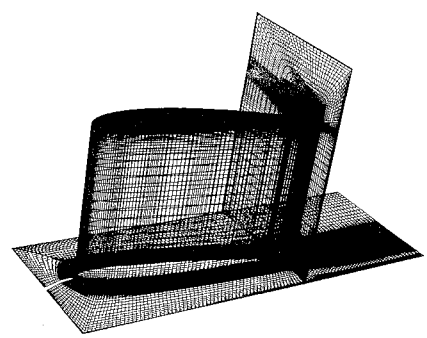

Fig. 2 Grid topology (grid size of 115 × 157 × 83).

grid near the wind-tunnel walls (generated using GRIDGEN2D[12]). The inner and outer two-dimensional grids were concatenated and smoothed out at the interface to form a single two-dimensional grid. The three-dimensional (volume) grid was then generated by stacking two-dimensional grids along the straight section of the wing and wrapping the grid around the rounded wing tip. The volume grid was made to conform to the wind-tunnel wall geometry by stretching and interpolation. The complete geometry case was computed using a grid (see Fig. 2) of size $115 \times 157 \times 83$, in the streamwise, spanwise, and surface-normal directions, respectively (ψ, η, and ζ directions of the curvilinear coordinate system). Of the 115 grid points streamwise, 40 were used in the wake region. Viscous grid spacing of $1 \times 10^{-3}c$ was imposed at the root wall, and on the other three wind-tunnel walls, a viscous spacing of $1 \times 10^{-4}c$ was used. Viscous grid spacing of $1 \times 10^{-6}c$ was specified on the wing surface, but this spacing was linearly expanded to $1 \times 10^{-5}c$ at the trailing edge and $1 \times 10^{-3}c$ at the outflow wake line. In the vortex core, a grid spacing of $5 \times 10^{-3}c$ was used. This core grid spacing was chosen based on the results of a grid refinement study using an analytical vortex (discussed further in a later section).

Turbulence Modeling

Turbulence models of varying levels of complexity have been used to study vortical flows. The Baldwin–Lomax algebraic turbulence model has been widely implemented for complex flow problems. However, it has severe limitations when applied to vortical flows because of difficulties in the definition of an unambiguous wall-algebraic length scale. Furthermore, models of this type do not take into account the transport and diffusion of turbulence, and so turbulence history effects are not captured. These effects are important for wingtip flows, recirculating flows, and separated flows.[13] Higher levels of turbulence modeling, such as one-equation models or two-equation models, likewise have deficiencies but are favored because they are thought to have a greater potential to characterize the physics of the tip vortex flow.

In the current study, a modified form of the Baldwin–Barth one-equation turbulence model[14] was used. The model can be implemented in a straightforward manner because there is no need to define an algebraic length scale. Simple turbulence models of this type overpredict the level of eddy viscosity in the core of a vortex. This shortcoming can be worked around through modification of the production term. In the standard Baldwin–Barth one-equation model, the production term P of νR_τ is approximated by

$$P = C_1 \nu R_\tau S \tag{1}$$

where C_1 is a constant, ν is the laminar viscosity, R_τ is the turbulent Reynolds number, and S is a scalar measure of the deformation tensor. There are several choices for S including basing S on the magnitude of vorticity, $|\omega| = (2\Omega_{ij}\Omega_{ij})^{1/2}$ (Ω_{ij} being the vorticity tensor,) on the strain rate $|s| = (2S_{ij}S_{ij})^{1/2}$ or on the norm of the entire tensor $(U_{ij}U_{ij})^{1/2}$ as discussed in Ref. 15. The option of basing S on $|\omega|$ is the simplest to implement, and it has a theoretical motivation in that turbulence is found where vorticity is generated (near solid boundaries). The choice of basing S on $|s|$ goes back to the κ equation or the turbulent kinetic energy equation, which is more rigorously derived but not necessarily superior to the other options. A newly proposed form, as suggested by Spalart,[16] combines $|\omega|$ and $|s|$ as follows:

$$P = C_1 \nu R_\tau (|\omega| + 2\min(0, |s| - |\omega|)) \tag{2}$$

The advantage of this formulation is that the eddy viscosity is reduced in the regions where the vorticity exceeds the strain rate, such as in the vortex core where the pure rotation should suppress the turbulence. The modification is passive in thin shear layers where $|s|$ and $|\omega|$ are very close; therefore, it does not interfere with the validation of the model presented in Ref. 17. This modification represents an attempt to empirically adjust the production term for vortex-dominated flows. Note that the factor 2 in this equation is an arbitrary constant that can be adjusted depending on the amount of diffusion the turbulence model gives. The effect of using factors other than 2 will be discussed in a later section of this paper. The transition to turbulence on the wing surface was measured[4] and then was fixed by a trip strip located at an arc length of $s/c = 0.0417$ from the leading edge. Early computations showed that the flow that included transition to turbulence was no different from the flow that did not include transition (i.e., fully turbulent flow). As a result, all subsequent runs were made without allowing for transition. In the future, the effect of transition will be investigated.

Measurement Procedure

Research was conducted in the 32×48 in. low-speed wind tunnel at the Fluid Mechanics Laboratory of NASA Ames Research Center. Maximum freestream turbulence in the wind tunnel, as measured by hot-wire anemometer, is 0.15%. The half-wing model has a 3-ft span and 4-ft chord, with a NACA 0012 airfoil section and rounded tip. Angle of attack of the wing was set at 10 deg. The tests have been carried out at a tunnel reference speed of 170 ft/s giving a chord Reynolds number of 4.6×10^6—a representative Reynolds number for a real-life helicopter blade at a subcritical Mach number or small aircraft wings. A trip was used to fix transition near the leading edge.

Glass-bead roughness elements of 0.017-in. diam were packed closely together to form a 1/8-in.-wide strip. The strip was placed across the span of the wing at a distance of 2.0 in. from the leading edge (as measured along the surface). The trip extended around the tip and along the bottom surface of the wing. Napthalene sublimation and microphone techniques were used to confirm that the boundary layers were turbulent after the trip. Although the Reynolds number is high enough for transition to occur naturally, past experience has shown that trips are necessary to ensure repeatability of the results over experiments of long duration. The trip was placed at the approximate location of naturally occurring transition on the pressure side of the wing. A seven-hole pressure probe was used to measure the velocity and pressure. On the upper half of the wing model surface, 222 static pressure taps were located in 12 chordwise rows. The absolute positioning accuracy of the seven-hole probe in the plane normal to the freestream direction was within 0.005 in. Wind-induced mean deflection of the probe stem in the streamwise direction could be as much as 0.045 in. depending on the length of exposed stem. To get a qualitative picture of the skin-friction lines on the wing, surface oil flow visualization was done using a mixture of titanium oxide, oleic acid, kerosene, 10 weight oil, and fluorescent powder, and photographed using a 2×2 in. large format still camera. An ultraviolet lamp was used to illuminate the mixture. Measurements were made at 11 stations between the leading edge and a point 0.67 chords downstream of the trailing edge, together with one plane at the wind-tunnel contraction exit, (0.15 chords upstream of the leading edge) to provide entry conditions for computations. The seven-hole probe measurement grids (in the $y-z$ plane) contained 609 points, with the closest spacing in the wing boundary layer and the vortex core.

Boundaries of the data planes were at $z/c = 0.27$, $z/c = 0.9$, $y/c = -0.24$, and $y/c = 0.24$ (see Fig. 1 for the wind-tunnel fixed coordinate system; x, y, z). Calibration of the seven-hole probe was done in situ before installation of the model. The procedure for the calibration is described in Ref. 18. For high flow angles (>30 deg), flow angle measurement uncertainty for the seven-hole probe is within 1 deg, whereas velocity magnitude uncertainty is within 1% of freestream velocity. For low flow angles (<30 deg), flow angle uncertainty is within 0.5 deg, whereas velocity magnitude uncertainty is within 0.8%. The effect of velocity gradients on the pressure probe results is minimal (0.1%). Data acquisition was done using a 32-bit DEC μVAX II computer to control a 15-bit Tustin X-2100 A/D. Measurement error due to A/D resolution was negligible compared with instrument error. A majority of the data is presented in Cartesian coordinates. This may not seem to be a good choice given that most past studies of vortices have used cylindrical polar coordinates. The deciding factors in the coordinate system choice were the fact that most Navier–Stokes computer codes are written using Cartesian coordinates and also, since the current vortex is still developing (not axisymmetric), not much is gained by using a different coordinate system. The processed data were displayed as color plots, of contours and otherwise, produced by the

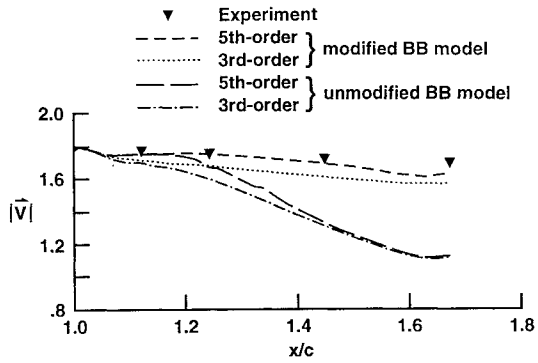

Fig. 3a Peak velocity magnitude at vortex core.

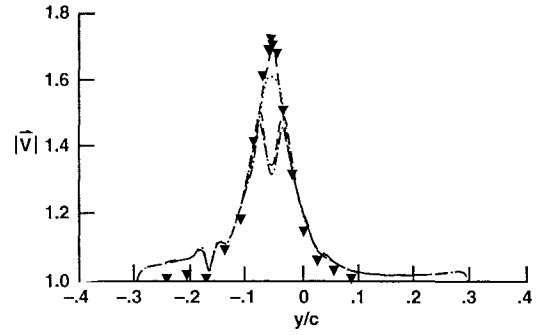

Fig. 3b Total velocity magnitude across vortex core at $x/c = 1.241$.

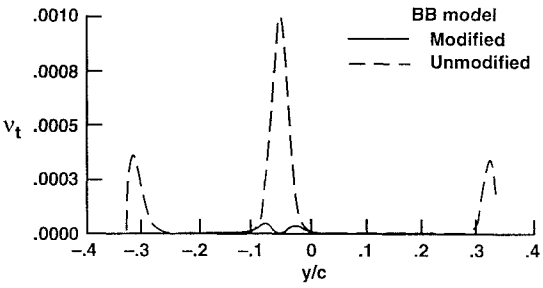

Fig. 3c Eddy viscosity profile across vortex core at $x/c = 1.241$.

software package FAST (Flow Analysis Software Toolkit), a suite of programs developed at NASA Ames.[19]

III. Results

During the course of this research project, a substantial amount of measured and computed results have been acquired. In the following sections, only a small selection of experimental results will be presented for comparison with the latest computation. The reader is encouraged to refer to previously published papers[4,20–22] for further information.

Wake Case

As discussed previously, an attempt was made to isolate undesired grid effects from the turbulence modeling questions. In addition to grid refinement studies performed using Rott's vortex, a second approach taken to isolate the grid effects was to turn the turbulence model off while leaving the molecular viscosity on. Grid refinement was then performed for this case.[21] Note that since measured inflow boundary conditions were used, these laminar computations were still a reasonable model problem of the vortex generated by the complete configuration (for studies of grid refinement, grid distribution, and other numerical issues). Finally, wake-case solutions were obtained using the Baldwin–Barth turbulence model implemented with two variations of the approximation of the production term.

Early on in the study, it was found that the third-order accurate differencing scheme for the convective terms of the momentum equations was too dissipative for the flow conditions specified. Presented in Fig. 3 is a comparison of third-order and fifth-order accurate differencing on the solution for a wake-case grid having 371,000 points ($35 \times 103 \times 103$). Note the high level of velocity at the core. This velocity excess is a characteristic of strong vortices in their early stages of development as explained in Ref. 20. Also shown in this figure is a comparison of the effects of the Baldwin–Barth turbulence model production term modification. One can see that the turbulence model modification has the greatest effect on the velocity at the core center, but this modification alone was not sufficient. An additional 5% improvement was obtained through application of fifth-order convective term differencing. The higher order differencing causes a reduction of the numerical dissipation caused by truncation of the convective terms. This represents a substantial improvement at little cost because the additional terms were added explicitly to the right-hand side of the finite difference Navier–Stokes equations (banded matrix remained the same size). In Fig. 3b, the core center velocity is underpredicted by roughly 25% for the cases with no turbulence model modification. In fact, for these cases, the velocity at the center of the core is less than that found in the outer portion of the core. Figure 3c illustrates the effect that the Baldwin–Barth turbulence model modification has on the eddy viscosity found in the vortex core. Notice how the results for the unmodified Baldwin–Barth model show a high level of eddy viscosity at the vortex core center. This result was contrary to what was observed in the experiment and indicated that the unmodified model was too diffusive in the vortex core and is what prompted the turbulence model modification. The improvements obtained by these modifications are very significant, but the results are still not completely free of error (caused by the numerics and the model), at the center of the vortex core.

Analytical Vortex Case

It is well known that proper grid resolution of the vortex core is crucial to compute the correct growth rate of a vortex. Unfortunately, limited computational resources (available computer memory) make the performance of a comprehensive grid refinement study unachievable at this time.

In the current study, grid refinement tests were performed on a model problem that used the analytical three-dimensional vortex solution derived by Rott[5] as the basis of comparison. Since Rott's analytical solution is for an isolated free vortex (no wing), the approach taken was to find an effective Reynolds number that would produce a similar inflow velocity profile (and hence similar circulation level) to that of the experiment. Upon doing so, the code was run laminar using this effective Reynolds number. The solutions were obtained using fifth-order accurate upwind-biased differencing of the convective terms. Four grids of size 7,056 ($16 \times 21 \times 21$), 26,896 ($16 \times 41 \times 41$), 59,536 ($16 \times 61 \times 61$), and 104,976 ($16 \times 81 \times 81$) points and of uniform grid spacing were generated.

Presented in Figs. 4a and 4b are the total velocity and crossflow velocity magnitude ($\sqrt{v^2 + w^2}$), respectively (note: $r_c \approx 0.035c$ of the full geometry problem). As can be seen in these figures, grid independence was achieved for the two finer grids (in Fig. 4, $\Delta y1'$ refers to the 7056-point grid etc.). The grid refinement study shows that an average of 15–20 grid points (in each of the crosswise and spanwise directions) in the viscous core region are needed to adequately resolve the flow. It was also determined that the vortex is more sensitive to crossflow plane grid refinement than streamwise refinement. At this point, one can say for the grid spacing of $\Delta y' = \Delta z' = 5 \times 10^{-3}c$ or finer (where x', y', and z' represent the analytical vortex coordinate system), the combined effect of the laminar viscosity and the numerical diffusion is of the same order of magnitude or less than that of the turbulent viscosity.

Complete Geometry Case

Computations of the complete geometry case, which we now present, included fifth-order accurate upwind-biased differencing of the convective terms, the modified Baldwin–Barth turbulence model, and a maximum grid spacing of 15 points across the core. To reduce the stiffness of the equations the pseudo-time step was set to $\Delta t = 10^6 c/U_\infty$. The code converged five orders of magnitude and required 180 μs/grid point/iteration (approximately 26 CPU h) on a Cray Research Corporation C-90 machine. Through preliminary computations of the complete geometry and analytical vortex cases, several grid distribution criteria emerged. To achieve the accuracy

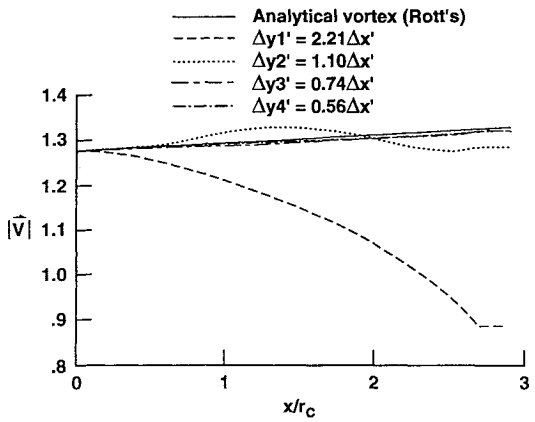

Fig. 4a Peak velocity magnitude at vortex core.

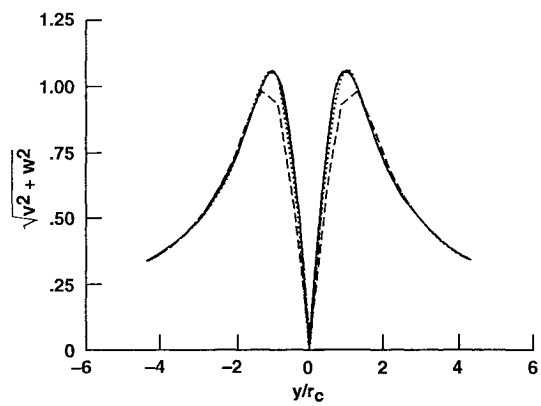

Fig. 4b Crossflow velocity magnitude across vortex core.

level of the current complete geometry results, a grid cell aspect ratio of 1 was required in the vicinity of the vortex core. Away from the core (on the inboard portion of the wing), the grid aspect ratio was as high as 100 and as high as 10,000 in the boundary layer. It was found (using the analytical vortex case) that a minimum of 15–20 grid points across the core were required to resolve the high velocity gradients (see Fig. 4a). Additionally, the y^+ of the first grid point above the wing surface was between 0.16–0.36. It should be noted that in practical applications a multizone grid would probably be used; therefore, although these general guidelines still apply, fewer total grid points would be needed to obtain comparable accuracy.

Presented in Fig. 5 is a comparison of the computed and measured velocity magnitude (measured by seven-hole pressure probe). The black outline in both figures represents the outer boundary of the measured planes. The first sign of the vortex rollup can be seen in the furthest upstream plane. At the trailing edge, the circulation of the vortex is 87% of its final level.[22] Notice also that the root vortex (low-momentum region) was captured by the computation designated here by the blue patch on the root wall. A closeup of the vortex (see Fig. 6) at $x/c = 0.803$ shows the details of the free-shear-layer detachment. It can be seen that the trends agree well, yet some of the finer details of the experiment are not accurately predicted. In both the computed and measured results, the shear layer detachment point is on the suction side of the wing tip. This result was expected because of the ability of turbulent boundary layers to withstand limited adverse pressure gradients. Recent trials of other turbulence models have shown that the flow in this vicinity is significantly affected by the choice of turbulence models.

The surface pressure contour comparison is shown in Fig. 7. The general trends and pressure levels of the computed and measured results agree well. Of particular interest is the pressure peak induced by the presence of the vortex above the suction side of the wing (green patch on the outboard portion of the wing near the trailing edge). In previous computational studies,[2] the magnitude and extent of this pressure region have been underpredicted due to lack of grid resolution and improper turbulence modeling. Although there are some differences, a chordwise line plot of C_p, or the pressure

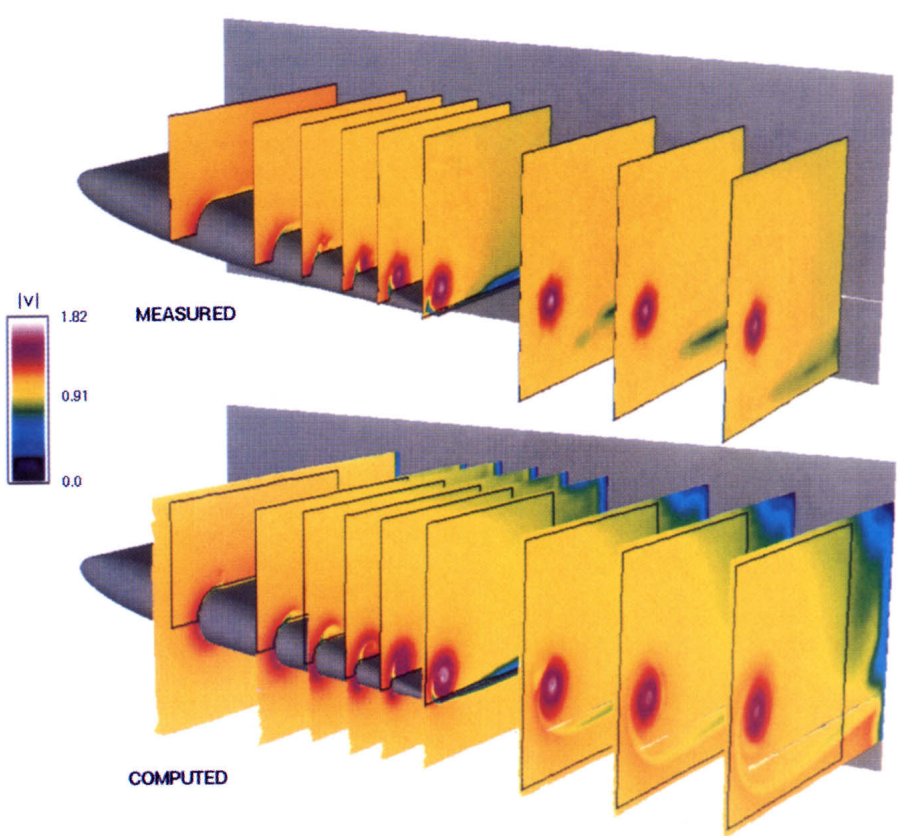

Fig. 5 Velocity magnitude contours.

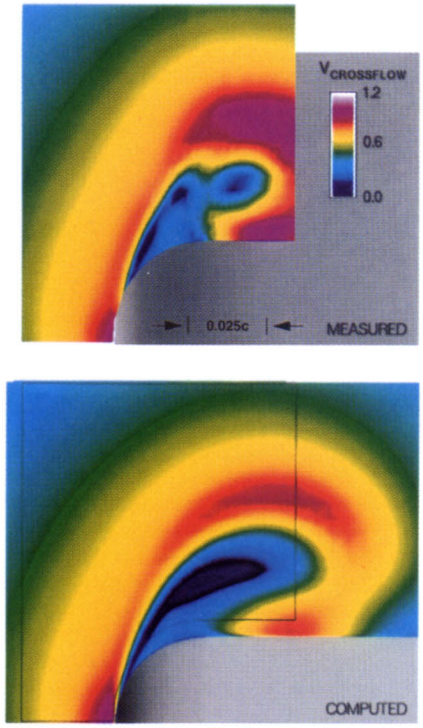

Fig. 6 Crossflow velocity at $x/c = 0.803$.

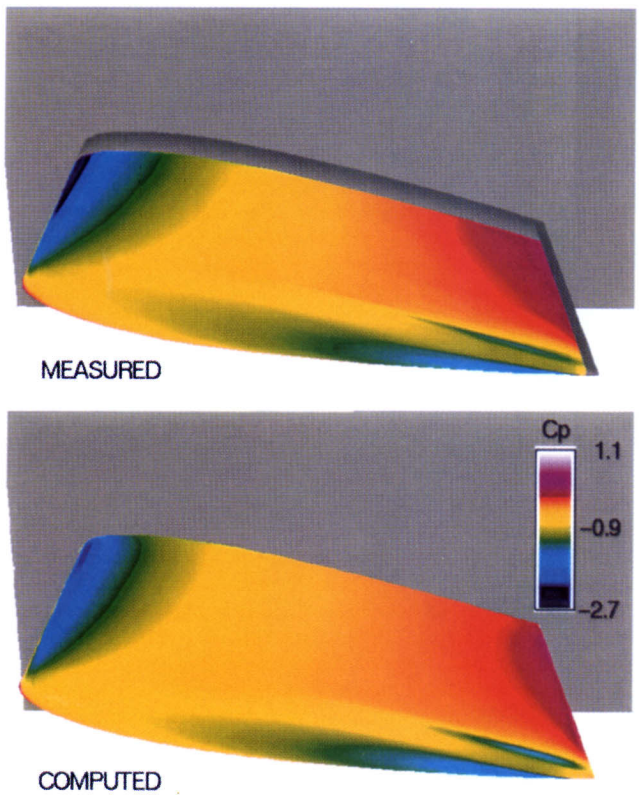

Fig. 7 Surface static pressure contours.

coefficient (located roughly under the vortex at $z/c = 0.667$) shown in Fig. 8, indicates that the vortex-induced peak is captured well by the computation.

An important measure of the validity of a Navier–Stokes computation is whether the surface skin-friction topology is computed correctly. Shown in Fig. 9 is a comparison of computed suction-side surface-particle trajectories superimposed on the surface skin-friction magnitude compared with the results of an oil-flow wind-tunnel experiment. As seen in this figure, the location and extent of the primary and secondary convergence lines agrees well with those of the experiment. The lower surface boundary layer flows around the tip to a line of surface streamline confluence or convergence as indicated by the dark grey particle lines. The convergence line is indicative of the departure of the shear layer from the surface and occurs as the fluid, moving in a crossflow direction, encounters an adverse pressure gradient. Near the rear of the wing tip a second convergence line, indicating the presence of a secondary vortex, is shown in the experiment and computation (light grey lines). On the suction-side midspan region of the wing, the computation shows a small area of separation near the trailing edge. As shown by the skin-friction magnitude level, the shear is low upstream of this region. Although not readily visible, this behavior is similarly reflected in the oil-flow pattern.

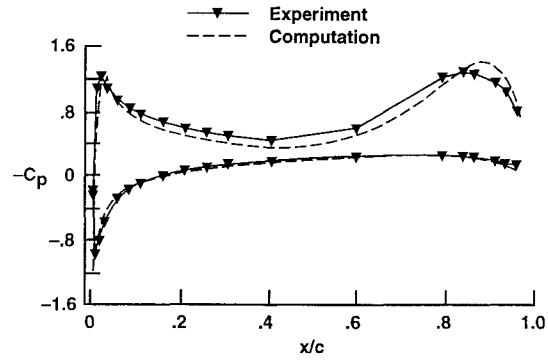

Fig. 8 Surface static pressure profile at $z/c = 0.667$.

The treatment of the outflow boundary condition has been of concern since early on in this study. Previous results [21] were computed using an experimentally measured pressure profile imposed at the exit (Dirichlet condition,using the experimentally measured pressure). These results showed a jump in the flow quantities close to the exit plane. It has been determined that this jump was caused by the tendency of the computed vortex to take a slightly different path (differs by up to $0.01c$) from that of the experiment. As a consequence of the extremely high gradients in the vicinity of the core, any slight mismatch in the core position (owing to numerical or experimental errors) can greatly affect the computed core flow near the outflow boundary. As a result, a Neumann boundary condition, which is a less restrictive condition than a Dirichlet condition, was used. The Neumann boundary condition is implemented such that the experimentally determined pressure gradient is prescribed at the outflow.

It was found, as shown in Fig. 10, that use of the Neumann condition significantly minimized the jump. It was also determined that this jump could be completely eliminated by using a Neumann condition calculated from the results of a previous solution (as opposed to a condition determined from measured results). However, this caused the tip vortex core velocity level upstream of the exit to be underpredicted. Figures 10a and 10b show comparisons of the experimental results with the computed results in the center of the vortex core. The maximum difference between experiment and computation in core-centerline velocity is approximately 3%, and this difference is observed near the outflow. Downstream of the trailing edge, diffusion causes the velocity magnitude at the core to decrease slowly as also is shown in the experimental results. As seen in these figures, results that used the experimentally determined Neumann outflow pressure boundary condition compared most favorably with the experiment; thus, this boundary condition was used for the remainder of the study.

The modified Baldwin–Barth turbulence model was implemented using several values for the constant C_1 other than 2. It was found that a value of 3.5–4.0 produced the best agreement with the experiment. Presented in Fig. 10b is the streamwise variation of the core static pressure. This comparison is the poorest of all of the quantities studied. It is interesting that it is possible to obtain a reasonable prediction of the core axial velocity yet significantly underpredict the magnitude of the static pressure. Since the vortex core approaches that of pure rotation, inviscid reasoning using Bernoulli's equation ($U = \sqrt{1 - C_p}$) shows that a 3% error in velocity (worst core velocity agreement with experiment) can cause a 9% error in static pressure. Since the core is viscous (and turbulent) and the static pressure disagreement is up to 25%, this is not a fully satisfactory explanation.

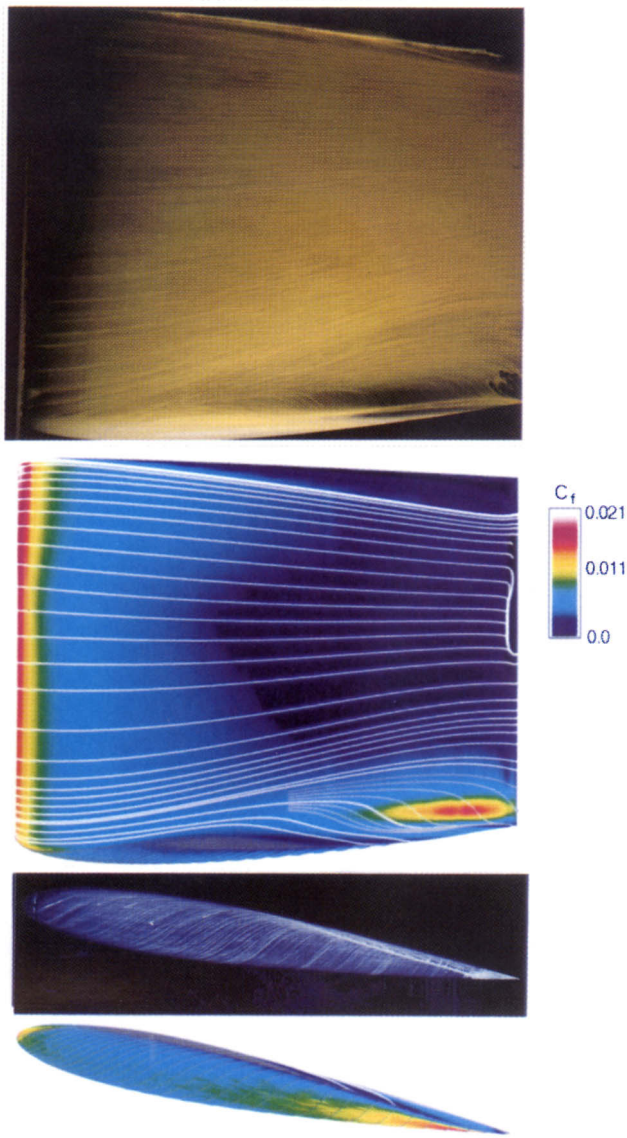

Fig. 9 Comparison of oil-flow pattern with computed surface particle pathlines.

A possible scenario is that the turbulence model is causing the discrepancy in core static pressure. This is likely to be the case because it appears that the radial momentum equation is satisfied as evidenced by the close agreement of the calculated and measured velocity distributions. A contributing factor to the core-static pressure underprediction is a poor representation of the normal Reynolds stresses typical of one-equation turbulence models. In one-equation models, it is expected that the pressure will be too high in some regions (but not the wall pressure) even though the velocity is accurate. This explanation can account for a few percent of the core-static pressure discrepancy.

One point to note is that there could be some effect of compressibility in the core. The maximum axial velocity measured in the core is 1.77 U_∞ ($M_\infty = 0.27$), which is in the range of slight compressibility. Here U_∞ is the freestream velocity and M_∞ is the freestream Mach number. An estimate of the effect of compressibility on the seven-hole probe velocity measurements shows that the maximum core-velocity magnitude would change by 0.2% if a compressible measurement technique was used.

Figure 11 shows a plot of the crossflow velocity distribution comparison in a plane near the outflow boundary plotted using a polar-cylindrical coordinate system with origin at the core center (the usual system used for vortices in the far field). The majority of the apparent scatter in the data is not error. The scatter arises from a combination of the asymmetry of the data and the fact that the experimental data were acquired on a rectangular grid and the computational data using a generalized coordinate system. Of importance in Fig. 11 is the

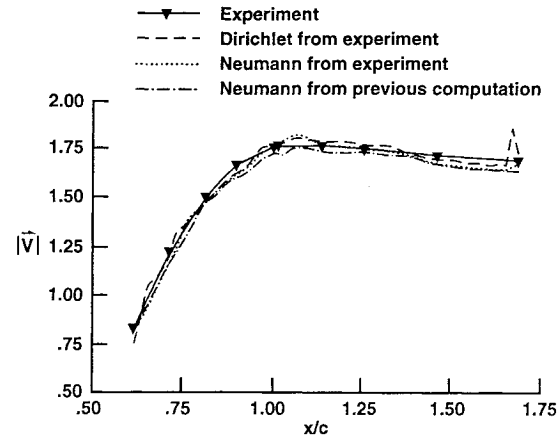

Fig. 10a Peak velocity magnitude at vortex core for different outflow boundary conditions.

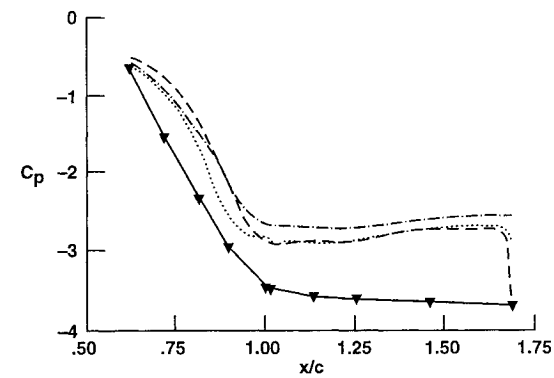

Fig. 10b Static pressure at vortex core for different outflow boundary conditions.

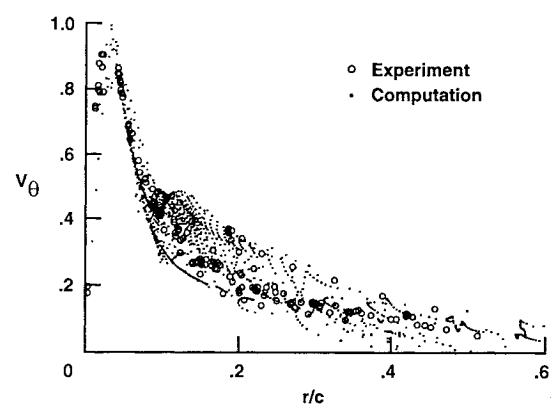

Fig. 11 Circumferential velocity at $x/c = 1.462$ plotted in polar-cylindrical coordinate system.

slight underprediction of the core radial crossflow velocity gradient (dv_θ/dr), which in turn greatly modifies the peak axial velocity found in the centerline of the core.[22] It is thought that additional improvements in the turbulence model would remedy this discrepancy.

IV. Conclusions

The formation and near-field roll-up of a turbulent wing tip vortex have been studied computationally and experimentally in an interactive fashion. In this study, the effects of inaccuracies due to numerics and turbulence models were addressed through an extensive validation process. Some important findings from this study include the following:

1) Fifth-order accurate upwind-biased differencing of the convective terms was found to be essential in reducing numerical dissipation and achieving reasonable agreement with measured vortex velocity profiles.

2) Grid independence for Rott's analytical vortex problem was achieved using a grid spacing of $\Delta(z'/r_c) = \Delta(y'/r_c) =$

$0.74\Delta(x'/r_c)$ or smaller, which is equivalent to $5 \times 10^{-3}c$ or smaller. Although it was not possible to prove conclusively that the complete geometry case was free of significant grid-related errors, this is likely to be the case because a similar level of resolution was used.

3) The production term in the Baldwin–Barth one-equation model was modified to suppress excessive diffusion of the vortex caused by the turbulence model. The results showed an improvement in the prediction of the viscous vortex core over the unmodified version.

4) Good agreement with measured results was found using 1.5 million grid points and the modified Baldwin–Barth one-equation model. Velocity profiles through the vortex compared to within 3% to the experiment. The core static pressure was underpredicted, which may be attributed to a deficiency in one-quation turbulence models. The occurrence of a secondary vortex has also been computed.

5) Use of a Neumann outflow pressure boundary condition was found to be preferable to a Dirichlet condition.

Future improvements in the computational results could be obtained by the incorporation of a turbulence model of greater sophistication. The measured near-field Reynolds stress distribution[22] shows that a turbulence model that uses a constant or isotropic eddy viscosity approach is not likely to be fully successful. Commonly used eddy-viscosity-based models have no way of reproducing the stabilizing effects of solid body rotation (except in an empirical manner similar to the one we used), but more advanced models are also likely to be deficient in this respect, judging by their general inability to predict the effects even of mild streamline curvature. It seems unlikely that anything simpler than a k-ε model or a full Reynolds-stress model has any hope of predicting the flow to within 0.5% accuracy.

Acknowledgments

The authors would like to thank Dochan Kwak, Philippe Spalart, and Stuart Rogers for their helpful discussions and comments on this research project.

References

[1]Mansour, N. N., "Numerical Simulation of the Tip Vortex of a Low-Aspect Ratio Wing at Transonic Speed," *AIAA Journal*, Vol. 23, No. 8, 1985, pp. 1143–1149.

[2]Srinivasan, G. R., McCroskey, W. J., Baeder, J. D., and Edwards, T. A., "Numerical Simulation of Tip Vortices of Wings in Subsonic and Transonic Flows," *AIAA Journal*, Vol. 26, No. 10, 1988, pp. 1153–1162.

[3]Spivey, W. A., and Morehouse, G. G., "New Insights into the Design of Swept-Tip Rotor Blades," 26th Annual National Forum of the American Helicopter Society, Paper 420, June 1970.

[4]Chow, J. S., Zilliac, G. G., and Bradshaw, P., "Initial Roll-Up of a Wingtip Vortex," *Proceedings of the Aircraft Wake Vortices Conference*, Vol. 2, Federal Aviation Administration, Washington, DC, 1991, pp. 35-1–35-17.

[5]Rott, N., "On the Viscous Core of a Line Vortex," *Journal of Applied Mathematics and Physics*, Vol. 9b, No. 5/6, 1958, pp. 543–553.

[6]Rogers, S. E., Kwak, D., and Kiris, C., "Steady and Unsteady Solutions of the Incompressible Navier–Stokes Equations," *AIAA Journal*, Vol. 29, No. 4, 1991, pp. 603–610.

[7]Rogers, S. E., "Progress in High Lift Aerodynamic Calculations," AIAA Paper 93-0194, Jan. 1993.

[8]Kiris, C., Chang, L., Kwak, D., and Rogers, S. E., "Incompressible Navier–Stokes Computations of Rotating Flows," AIAA Paper 93-0678, Jan. 1993.

[9]Chorin, A. J., "A Numerical Method for Solving Incompressible Viscous Flow Problems," *Journal of Computational Physics*, Vol. 2, No. 1, 1967, pp. 12–26.

[10]Rai, M. M., "Navier–Stokes Simulations of Blade–Vortex Interaction Using High-Order Accurate Upwind Schemes," AIAA Paper 87-0543, Jan. 1987.

[11]Chan, W., Chiu, I., and Buning, P., "User's Manual for the HYPGEN Hyperbolic Grid Generator and the HGUI Graphical User Interface," NASA TM 108791, Oct. 1993.

[12]Steinbrenner, J., Chawner, J., and Fouts, C., "The GRIDGEN 3D Multiple Block Grid Generation System," User's Manual, Interim Rept., Vol. 2, MDA Engr. Inc., Arlington, TX, Oct. 1987–Oct. 1990.

[13]Menter, F., "Performance of Popular Turbulence Models for Attached and Separated Adverse Pressure Gradient Flows," *AIAA Journal*, Vol. 30, No. 8, 1992, pp. 2066–2072.

[14]Baldwin, B. S., and Barth, T. J., "A One-Equation Transport Model for High Reynolds Number Wall-Bounded Flows," NASA TM 102847, Aug. 1990.

[15]Spalart, P. R., and Allmaras, S. R., "A One-Equation Turbulence Model for Aerodynamic Flows," AIAA Paper 92-0439, Jan. 1992.

[16]Spalart, P. R., private communication, Boeing Corp., 1993.

[17]Baldwin, B. S., and Barth, T. J., "A One-Equation Transport Model for High Reynolds Number Wall-Bounded Flows," AIAA Paper 91-0610, Jan. 1991.

[18]Zilliac, G. G., "Modeling, Calibration and Error Analysis of Seven-Hole Pressure Probes," *Experiments in Fluids*, Vol. 14, No. 2, 1993, pp. 104–120.

[19]Walatka, P. P., Plessel, T., McCabe, R. K., Clucas, J., and Elson, P. A., "FAST User's Manual," NASA Internal Rept., Sept. 1991.

[20]Chow, J. S., Zilliac, G. G., and Bradshaw, P., "Near-Field Formation of a Turbulent Wingtip Vortex," AIAA Paper 93-0551, Jan. 1993.

[21]Dacles-Mariani, J., Rogers, S., Kwak, D., Zilliac, G. G., and Chow, J. S., "A Computational Study of a Wingtip Vortex Flowfield," AIAA Paper 93-3010, June 1993.

[22]Zilliac, G. G., Chow, J. S., Dacles-Mariani, J., and Bradshaw P., "Turbulent Structure of a Wingtip Vortex in the Near Field," AIAA Paper 93-3011, July 1993.

Color reproduction courtesy of the NAS Graphics Lab, NASA